Journal of Hazardous Materials 183 (2010) 381–388

Contents lists available at ScienceDirect

Journal of Hazardous Materials

journal homepage: www.elsevier.com/locate/jhazmat

The effect of carbon type on arsenic and trichloroethylene removal capabilities of iron (hydr)oxide nanoparticle-impregnated granulated activated carbons

Anne Marie Cooper[a,1], Kiril D. Hristovski[b,*], Teresia Möller[c,2], Paul Westerhoff[d,3], Paul Sylvester[c,2]

[a] Environmental Technology, College of Technology and Innovation. Arizona State University – Polytechnic Campus, 6075 South Williams Campus Loop West, Mesa, AZ 85212, United States
[b] Environmental Technology, College of Technology and Innovation, Arizona State University – Polytechnic Campus, 6073 South Backus Mall, Mesa, AZ 85212, United States
[c] SolmeteX – Division of Layne Christiansen, 50 Bearfoot Road, Northborough, MA 01532, United States
[d] School of Sustainable Engineering and the Built Environment, Arizona State University, Box 5306, Tempe, AZ 85287-5306, United States

ARTICLE INFO

Article history:
Received 19 April 2010
Received in revised form 9 July 2010
Accepted 9 July 2010
Available online 16 July 2010

Keywords:
Arsenic
Nanoparticle
Iron (hydr)oxide
GAC
Adsorption
Trichloroethylene
Water treatment

ABSTRACT

This study investigates the impact of the type of virgin granular activated carbon (GAC) media used to synthesize iron (hydr)oxide nanoparticle-impregnated granular activated carbon (Fe-GAC) on its properties and its ability to remove arsenate and organic trichloroethylene (TCE) from water. Two Fe-GAC media were synthesized via a permanganate/ferrous ion synthesis method using bituminous and lignite-based virgin GAC. Data obtained from an array of characterization techniques (pore size distribution, surface charge, etc.) in correlation with batch equilibrium tests, and continuous flow modeling suggested that GAC type and pore size distribution control the iron (nanoparticle) contents, Fe-GAC synthesis mechanisms, and contaminant removal performances. Pore surface diffusion model calculations predicted that lignite Fe-GAC could remove ~6.3 L g^{-1} dry media and ~4 L g^{-1} dry media of water contaminated with 30 $\mu g\,L^{-1}$ TCE and arsenic, respectively. In contrast, the bituminous Fe-GAC could remove only ~0.2 L/g dry media for TCE and ~2.8 L/g dry media for As of the same contaminated water. The results show that arsenic removal capability is increased while TCE removal is decreased as a result of Fe nanoparticle impregnation. This tradeoff is related to several factors, of which changes in surface properties and pore size distributions appeared to be the most dominant.

1. Introduction

The availability of clean drinking water is a problem faced by developed as well as developing nations, as population growth has created a worldwide demand for new water sources [1]. Unfortunately, many potential water sources contain high levels of contaminants from natural and anthropogenic origins that are hazardous to human health. Arsenic is a naturally occurring water contaminant that can also occur as a result of anthropogenic activities [2]. Arsenic levels in fresh waters typically are below 10 $\mu g\,L^{-1}$, but can reach concentrations in excess of several hundred $\mu g\,L^{-1}$ [3]. Because of the known carcinogenicity and toxicity of arsenic, the United States Environmental Protection Agency (USEPA) has established a maximum contaminant level (MCL) of 10 $\mu g\,L^{-1}$ in drinking water [4,5]. Recent arsenic risk assessments suggest that this MCL may be further lowered to 0.1 $\mu g\,L^{-1}$ [5]. This new regulatory pressure may require revisiting old and developing new treatment approaches for arsenic removal. Adsorption of arsenic by metal (hydr)oxides has been shown to be effective in removing arsenic below the existing MCL [6–11]. This technology is especially suitable for small and portable point-of-use systems such as those found in small communities where energy-demanding conventional water treatment technologies are unavailable.

Water sources may also contain other contaminants that have different chemistries than arsenic. Organic chemicals, for example, can often be found in groundwaters, especially in areas affected by heavy industrial activity. Trichloroethylene (TCE) is a typical organic contaminant found in drinking water supplies because of metal degreasing activities [12]. The USEPA has established a drinking water MCL for TCE of 5 $\mu g\,L^{-1}$, which is even lower than that for arsenic [13]. The presence of multiple inorganic and organic co-contaminants in water sources, such as arsenic and TCE, can further complicate water treatment. However, TCE can be considered a model organic contaminant in this context because it does not interact with arsenate or compete for its adsorption sites as a result of its different chemistry.

* Corresponding author. Tel.: +1 480 727 1291; fax: +1 480 727 1236.
E-mail addresses: Anne.M.Cooper@asu.edu (A.M. Cooper), Kiril.Hristovski@asu.edu (K.D. Hristovski), tmoller@solmetex.com (T. Möller), p.westerhoff@asu.edu (P. Westerhoff), psylvester@solmetex.com (P. Sylvester).
[1] Tel.: + 1 480 727 1132.
[2] Tel.: +1 508 393-5115; fax: +1 508 393 1795.
[3] Tel.: +1480 965-2885; fax: +1 480 965 0557.

0304-3894/$ – see front matter © 2010 Elsevier B.V. All rights reserved.
doi:10.1016/j.jhazmat.2010.07.036

To effectively treat multiple contaminants with different chemistries, requires either implementation of a series of treatment trains, or a complete change in treatment technology. If adsorption is the treatment method of choice, adsorbents other than metal (hydr)oxides must be used because they are not suitable for treatment of organic contaminants. Granular activated carbon (GAC) effectively removes organic contaminants, but it is not suitable for treatment of inorganic contaminants such as arsenic. Recent studies, however, have shown that hybrid activated carbon media containing iron (hydr)oxide nanoparticles (Fe-GAC) can simultaneously remove arsenic and organics [11,14–16]. Based on previously published work, it is hypothesized that the type of virgin GAC (V-GAC) material may affect the arsenic and organic co-contaminant removal capabilities of these hybrid adsorbent media. Therefore, the goal of this study was to investigate how the type of GAC impacts iron based nanoparticle loading, and how these in-situ synthesized nanoparticles impact the overall arsenic and organic co-contaminant (TCE) removal from water. Based on the existing literature, investigations addressing these factors that could affect the performance of hybrid iron (hydr)oxide-GAC media have not been conducted.

To accomplish the goal of this novel investigation, bituminous and lignite-based GAC media were treated with permanganate and ferrous salts to synthesize iron (hydr)oxide nanoparticles in situ as described by Hristovski et al. [11,17]. To better understand the synthesis process, the major manganese species and their concentrations were tracked and their effect on Fe-GAC adsorption properties was investigated. Arsenic and TCE removal capabilities of the synthesized Fe-GAC were studied by conducting equilibrium batch adsorption tests. The obtained isotherm data was used to model adsorbents' performance in a full-scale continuous flow packed bed setting.

2. Experimental approach

2.1. Media synthesis

Table 1 summarizes the types and properties of the V-GAC used to synthesize the Fe-GAC media. Two types of commercially available virgin GAC materials (Norit Americas Inc., USA) were impregnated with iron (hydr)oxide nanoparticles using a synthesis method described by Hristovski et al. [11,17]. In brief, 50 g of air-dried virgin GAC were gently mixed with 500 mL of 0.2 M $KMnO_4$ for 15 min in a rotating mixer at 30 rpm. The permanganate pretreated media was then repeatedly rinsed with ultrapure water until the wash water did not exhibit any pink/purple color characteristic of permanganate. Next, the rinsed media was gently mixed with 500 mL of 1 M $FeSO_4{\cdot}7H_2O$ for 6 h on a rotating mixer at 30 rpm. During the iron (hydr)oxide formation process, Fe^{2+} is oxidized and forms FeOOH [11]. Protons generated during the process were neutralized by soaking and rinsing the media with 5% $NaHCO_3$ solution until complete acid neutralization was obtained. The media was then rinsed with ultrapure water (<1 $\mu S\,cm^{-1}$) and stored wet before use.

To better understand the role of the reactants in the formation and distribution of nanoparticles in the final product, manganese was tracked by (1) collecting the rinse water from each reaction step and analyzing for total manganese and permanganate and (2) collecting samples from the permanganate-treated GACs (Mn-GACs) and Fe-GACs. The obtained data was used to conduct a manganese mass balance.

2.2. Media characterization and analytical methods

The iron and manganese contents of the Fe-GAC and Mn-GAC samples were determined by acid digestion in concentrated HNO_3 and 30% H_2O_2 (US EPA SWA 846, Method 3050B) followed by flame-atomic absorption spectroscopy (Varian Spectra 50B) [18,19]. Before the acid digestion, samples were ground to a powder and dried at 104 °C to constant mass to remove any moisture. The permanganate concentration was measured using a UV/vis spectrophotometer (Jenway 6405, Barloworld Scientific Ltd., UK) according to Cairus Analytical Method 102 [20]. Arsenic was analyzed using a graphite furnace atomic absorption spectrophotometer (GF-AAS) Varian Zeeman Spectra 400. TCE was analyzed using solid phase micro extraction (SPME) method on a Varian Saturn 2100 GC/MS/MS.

The iron and manganese distributions throughout the Fe-GAC were evaluated by mapping energy dispersive X-ray (EDX) microanalysis (EDAX Inc.). The carbon samples were glued to an epoxy resin and sliced to reveal the inner core of the particle. Focused ion beam (FIB) and scanning electron microscopy (SEM) techniques were employed to determine the size and shape of the deposited iron (hydr)oxide nanoparticles within the pores of the media (Nova 200 NanoLab UHR FEG-SEM/FIB and XL 30 by FEI). A backscatter detector was used to differentiate the iron from the carbon inside the Fe-GAC. This backscatter detector differentiated between heavier elements such as iron, which appear as whiter areas, and lighter elements such as carbon, nitrogen, oxygen and hydrogen, which appear as darker areas.

The surface charges and isoelectric points of the particles were estimated by measuring the zeta potential (ZetaPALS, Brookhaven Instruments Corporation, Holtsville, NY) at different pH values in 10 mM KNO_3 background electrolyte solution. The solution pH was adjusted by the drop-wise addition of 1 and 0.1 M KOH or HNO_3. X-ray diffraction (XRD) spectra of the finely powdered samples of the virgin and Mn-GAC were analyzed using a high resolution X-ray diffractometer (PANalytical X'Pert Pro, CuKα source). The obtained spectra were compared with the existing library of spectra to identify the intermediate manganese species involved in nanoparticle formation. The density and porosity of all media in bulk were estimated following a procedure described in Sontheimer et al. [21]. Surface area and pore size distributions of the samples were measured using the Brunauer, Emmett, Teller (BET) method (Micrometrics Tristar-II 3020 automated gas adsorption analyzer).

2.3. Batch equilibrium adsorption tests

The arsenic adsorption capacity of the media was evaluated in batch arsenate adsorption experiments at two final pH values, 7.2 ± 0.1 and 8.0 ± 0.1 in 10 mM $NaHCO_3$ with an initial arsenate concentration of $C_0 \approx 120\,\mu g\,L^{-1}$. These two pH values were selected because (1) most natural waters exhibit pH in this range; and (2) the arsenate adsorption capacity is affected by pH due to the speciation of arsenic (protonation–deprotonation) and change

Table 1
Estimated properties of the four different types of GAC media used in this study.

Media name	Description	BET surface area (m^2/g)	Particle density (kg/m^3)	Iron content (%Fe in dry media)
Lignite V-GAC	Untreated lignite GAC	696 ± 5	~383	<0.2
BituminousV–GAC	Untreated bituminous GAC	847 ± 12	~408	<0.2
Lignite Fe–GAC	Lignite GAC containing FeOOH nanoparticles	572 ± 4	~421	~12.1
Bituminous Fe–GAC	Bituminous GAC containing FeOOH nanoparticles	742 ± 10	~427	~8.5

Table 2
Porosities, tortuosities, and pore diffusion coefficients for the virgin GAC samples and GAC media containing iron (hydr)oxide nanoparticles.

Media type	Particle porosity (ε_P)	Tortuosity (τ)	Pore diffusion coefficients	
			For arsenate $D_{P(As)}$ (cm^2/s)	For TCE $D_{P(TCE)}$ (cm^2/s)
Lignite V-GAC	0.65	2.80	3.61×10^{-6}	4.66×10^{-6}
Bituminous V-GAC	0.57	3.61	1.42×10^{-6}	3.61×10^{-6}
Lignite Fe-GAC	0.65	2.80	3.61×10^{-6}	4.66×10^{-6}
Bituminous Fe-GAC	0.57	3.61	1.42×10^{-6}	3.61×10^{-6}

in the surface charge of the adsorbent. The TCE adsorption capacity of the media was only evaluated at pH = 8.0 ± 0.1 because TCE exists as the same species over a wide pH range. The initial TCE concentration was $C_0 \approx 6\,mg\,L^{-1}$. This type of buffered water was selected as a model to eliminate possible interferences from other contaminants that may compete with arsenic or TCE for available sorption sites. Such interferences may prevent proper investigation of the factors related to adsorbent properties that impact arsenic and TCE removal.

Teflon-capped amber glass 250-mL bottles were used as reactors. Media dosages ranged from 0.005 to 0.6 g dry media L^{-1}. TCE loss was prevented by eliminating headspace in the reactors. Adsorption of both arsenate and TCE were modeled using the Freundlich isotherm model [22,23]:

$$q_e = K_A C_E^{1/n} \quad (1)$$

where q_e is adsorption capacity (mg adsorbate/g adsorbent), K_A is Freundlich adsorption capacity parameter (mg adsorbate/g adsorbent)(L/mg adsorbate)$^{1/n}$, C_E is equilibrium concentration of the contaminant in liquid-phase of solution (mg adsorbate L^{-1}), and *1/n* is Freundlich adsorption intensity parameter (unitless).

2.4. Modeling performance of a full-scale packed bed system for arsenic and TCE removal

The pore surface diffusion model (PSDM) was used to model, predict and compare the performance of full-scale fixed-bed systems packed with Fe-GAC media synthesized on two different carbon bases. This model was initially developed to predict the performance of adsorbent beds packed with GAC media designed to remove organic contaminants [21]. However, Hristovski et al. [24] validated its suitability for predicting arsenic breakthrough for this hybrid media. The estimates for the external mass transport coefficient (k_f) were based on the Gnielinski correlation

$$k_f = \frac{[1 + 1.5(1-\varepsilon)] \times D_l}{d_p} \times \left(2 + 0.644 \times Re^{1/2} \times Sc^{1/3}\right) \quad (2)$$

$$Re = \frac{\rho_l \times \Phi \times d_p \times v_l}{\varepsilon \times \mu_l} \quad (3)$$

$$Sc = \frac{\mu_l}{\rho_l \times D_l} \quad (4)$$

Constraints: $Re \times Sc > 500$; $0.6 \le Sc \le 10^4$; $1 \le Re < 100$; $0.26 < \varepsilon < 0.935$where k_f is the external mass transport coefficient (calculated $k_f \approx 6.83 \times 10^{-3}\,cm\,s^{-1}$ for arsenate; $k_f \approx 1.19 \times 10^{-2}\,cm\,s^{-1}$), *Re* is the Reynolds number (unitless), *Sc* is the Schmidt number (unitless), d_p is the adsorbent particle diameter ($d_p = 0.420 \times 10^{-3}$ m), D_l is the free liquid diffusivity for arsenate or TCE, ε is the bed void fraction ($\varepsilon = 0.3$), μ_l is the dynamic viscosity of water at 20 °C ($1.002 \times 10^{-3}\,N^{-2}$), ρ_l is the density of water at 20 °C ($\rho_l = 998.2\,kg\,m^{-3}$), Φ is the sphericity of the particle (assumed $\Phi = 1$), and v_l is the liquid superficial velocity ($v_l \approx 0.00319\,m^{-1}$).

For arsenate and TCE, liquid diffusivities of $D_l = 9.05 \times 10^{-10}$ and $D_l = 20.1 \times 10^{-10}\,m^2\,s^{-1}$, respectively, were used [25,26]. The modeled hypothetical packed bed had a diameter of 1 m and length of 2 m. The empty bed contact time (EBCT) was ~5 min at a loading rate of 10 GPM ft^{-2} (~406 L m^{-2} min^{-1}). The initial concentrations for arsenic and TCE were set at the very realistic 30 μg L^{-1} to allow for better comparison of the breakthrough curves.

Because the Fe-GAC media are very porous, pore diffusion was assumed to be dominant over surface diffusion for intraparticle mass transport, and the impact of surface diffusion was assumed to be negligible. The pore diffusion coefficient was estimated using Eq. (5) as suggested by Sontheimer et al. [21]:

$$D_P = \frac{\varepsilon_P \times D_l}{\tau} \quad (5)$$

The tortuosity was estimated using the correlation suggested by Mackie and Meares (Eq. (6)) [27]:

$$\tau = \frac{(2 - \varepsilon_P)^2}{\varepsilon_P} \quad (6)$$

where τ is the tortuosity factor and ε_P is the particle porosity. The estimated porosity and tortuosity parameters of the media are given in Table 2 together with the estimated pore diffusion coefficients for arsenic and TCE. It is interesting to note that the method suggested by Sontheimer et al. [21] did not reflect the actual changes in media's porosity before and after the synthesis. This is probably because the iron coating in the channels and pores changed the pore sizes very little relative to the macro pore size of the carbon (>200 nm), which mostly contributes to porosity estimates when bulk measurement methods are used. In reality, however, the change in the micropore and mesopore size distributions could slightly increase the tortuosity factor and negligibly impact the profile of the breakthrough curve. Since this study focuses on the adsorption capacities of the media as a measure of their performance, any impact of this minimal limitation can be completely neglected for this specific case. PSDM simulations were conducted using AdDesignS™ software (Michigan Technological University) [28].

3. Results and discussion

3.1. Media characterization

Prior to Fe-GAC synthesis, both types of virgin GAC media (lignite and bituminous) exhibited iron contents of <0.2% Fe per dry GAC weight. After Fe-GAC synthesis, the iron content of the lignite-based Fe-GAC was increased to ~12.1% Fe per dry GAC. The iron content of the bituminous Fe-GAC increased to ~8.5% Fe per dry GAC weight, which was about 30% lower than its lignite-based counterpart. This is interesting, as both media were synthesized using the same treatment method and under the same conditions. These findings imply that the type of GAC used as a base material has an impact on the overall iron content of the final synthesized media.

In contrast to the iron content, the type of GAC media did not seem to affect the morphology or the distribution of the iron (hydr)oxide nanoparticles significantly. FIB/SEM microscopy revealed the presence of berry-like nanoparticles inside the pores of both types of Fe-GAC media. The size of these nanoparticles ranged

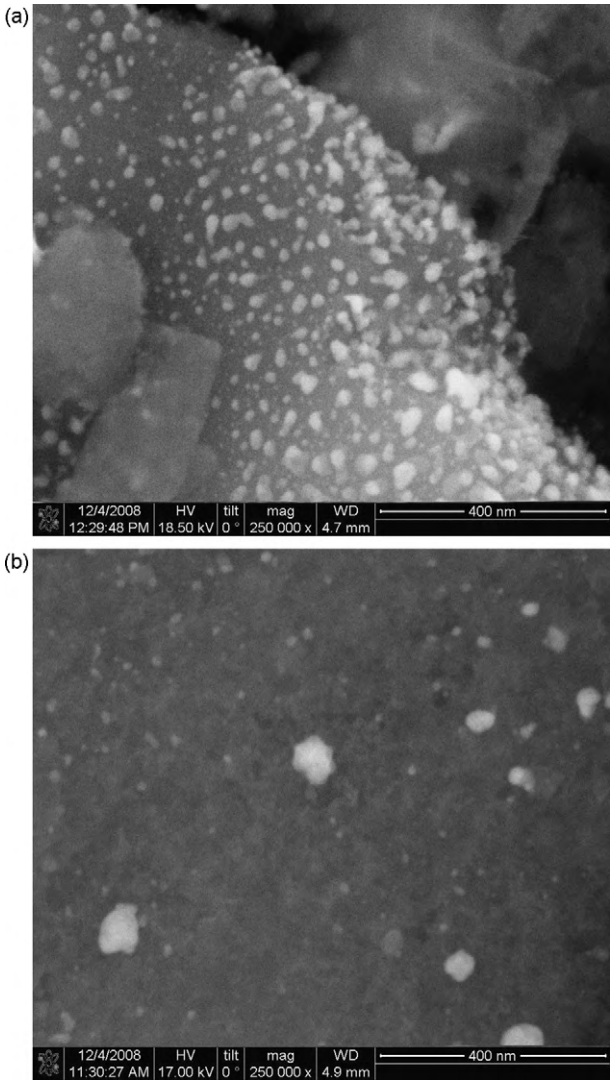

Fig. 1. (a) A high magnification FIB/SEM image confirms the presence of nanoscale iron (hydr)oxide nanoparticles in the synthesized bituminous Fe-GAC. (b) A high magnification SEM/FIB image shows nanoscale iron (hydr)oxide particles in the synthesized lignite-based Fe-GAC.

from ~10 to ~80 nm (Fig. 1). Particles were more concentrated in the outer regions of the media or its large pores, as illustrated for the lignite-based Fe-GAC in Fig. 2. These iron distribution patterns tend to coincide with the distribution of manganese in the Mn-GAC, implying that the manganese species present in the GAC after the permanganate pretreatment step control the formation of iron (hydr)oxide nanoparticles [11].

Table 1 summarizes the surface area results for the GAC samples before and after the synthesis. Samples with high iron content also exhibited a large decrease in surface area. The lignite-based Fe-GAC exhibited a ~17.9% (ΔSA = ~125 m^2/g) decrease in surface area after synthesis. In contrast, the bituminous Fe-GAC (with lower iron content) exhibited a ~12.4% (ΔSA = ~105 m^2/g) loss of its initial surface area. This relationship between decreased surface area and increased iron loading may be problematic in applications in which high surface area is an integral factor in the ability of the media to remove contaminants. The decrease in surface area also correlated well with the decrease in available mesopores and macropores, as illustrated by Fig. 3.

The formation of iron (hydr)oxide nanoparticles resulted in an increase in the isoelectric point of the Fe-GAC relative to the corresponding virgin media. This is expected, as iron (hydr)oxide and iron oxides have a high isoelectric point of $pH_{ZPC} \approx 8–9$ [29]. Such a high isoelectric point is favorable for media expected to remove a negatively charged oxo-ion, such as arsenate, in waters with pH ≥ 7. The lignite-based V-GAC and Fe-GAC media had lower isoelectric points than their bituminous counterparts (Fig. 4). Lower isoelectric points in GAC are consistent with a more oxidized surface and the presence of oxygen-containing functional groups, such as hydroxyl, carboxyl and carbonyl groups [21]. Furthermore, the presence of impurities such as silica, sulfur, and other contaminants in the GAC can also contribute to lower isoelectric points. These functional groups and impurities are more common in lignite-based GAC because lignite coal (the base material for producing lignite-based GAC) is a geologically younger material and is not exposed to the same reducing conditions and pressures as bituminous coal during the aging process [21,30].

3.2. The role of manganese species and pH in Synthesis of iron (hydr)oxide nanoparticles

Manganese species were tracked and a manganese mass balance was assessed throughout all synthesis steps to better understand the effect that GAC type had on manganese species involved in the formation of iron (hydr)oxide nanoparticles [11]. The degree of manganese loading of the GAC during the permanganate pretreatment has an impact on the final iron loading of the Fe-GAC media. Thus, the lignite-based GAC, which retained more manganese during the permanganate treatment, exhibited higher iron content than the bituminous GAC, as summarized in Table 3.

This table also lists the concentrations of permanganate and total manganese after each step of the synthesis process. During the permanganate pretreatment step, lignite-based Mn-GAC retained ~90% of the manganese from the initial permanganate solution, whereas the bituminous GAC retained ~75%. A possible explanation for the observed difference in these two media is that the permanganate more readily diffused and was retained in the lignite-based GAC pores due to its greater macroporosity. However, another possible explanation is that more permanganate was reduced to form less soluble manganese species, such as Mn(IV), which remained inside the lignite-based GAC after the permanganate treatment. This scenario is suggested by the very low percentage (~1%) of unreacted permanganate in the rinse solution after pretreatment of the lignite-based GAC. In contrast, almost one-fifth of the permanganate (~18%) was washed off the bituminous GAC in the rinse solution after the permanganate step, suggesting lower reactivity of this material with the strong oxidizer. This seems a reasonable explanation in the context that it is easier to further oxidize a partially oxidized surface (e.g., one that has more oxygen-containing functional groups such as lignite-based GAC) than it is to oxidize one that is not partially oxidized (such as bituminous GAC).

The XRD data (Supplemental Information Figure S1) seem to support these explanations. The presence of one strong peak at 27.3 two-theta degrees and the absence of any other peaks suggest the presence of an MnO_2 species (e.g., pyrolusite) in the permanganate-treated lignite-based GAC [31]. It contrast, the presence of two barely distinguishable peaks at 24.9 and 27.7 two-theta degrees in the XRD spectra suggest the presence of permanganate in the Mn–treated bituminous GAC. However, the low ratio of manganese species with respect to carbon and other species and the high background noise as a result of the heterogeneity of the GAC material may render these XRD spectra in need of additional support by data obtained using specialized analytical tools that were not available to the researchers.

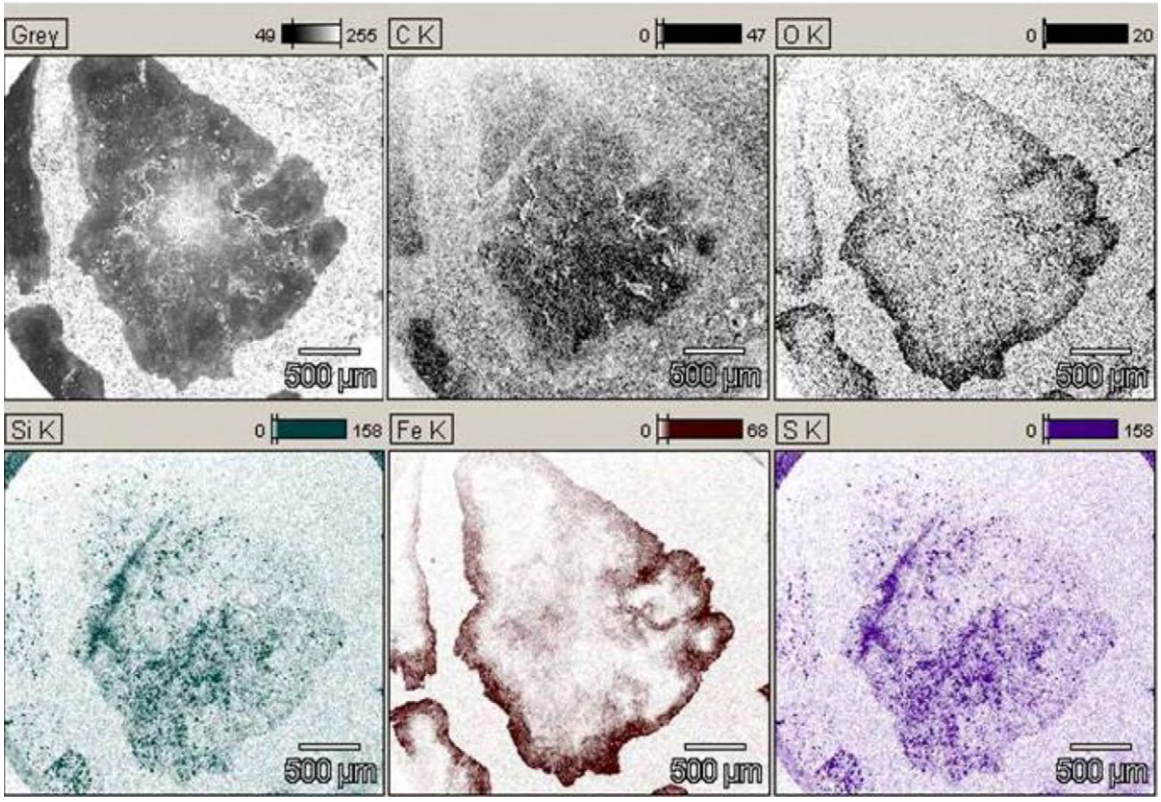

Fig. 2. Elemental distribution of carbon, iron, oxygen, silica, sulfur and manganese in lignite-based Fe-GAC.

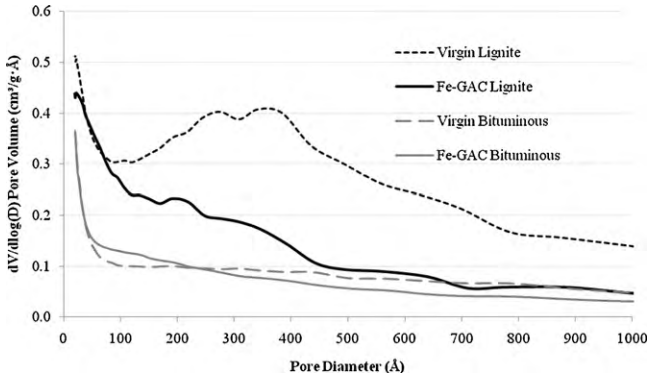

Fig. 3. Differential pore volume as a function of pore diameter for virgin and Fe-GAC samples.

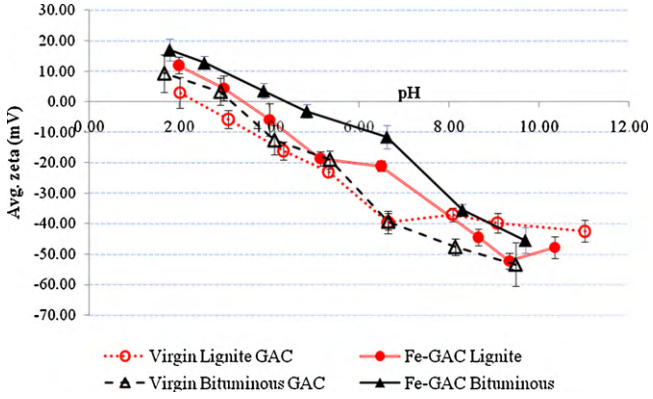

Fig. 4. Chart of isoelectric measurements for lignite and bituminous virgin and Fe-GAC. Error bars represent 95% confidence intervals.

The presence of two different Mn phases in the two intermediate Mn-GAC samples indicates that different intermediate steps may be involved in the formation of the iron (hydr)oxide nanomaterials in different base GAC media. The formation of these nanoparticles can be described as in Eqs. (7) and (8) [25,32,33]:

$$6H_2O + 5Fe^{2+} + MnO_4^- \rightarrow 5FeOOH \downarrow + 7H^+ + Mn^{2+} \quad \Delta G_f^\circ = -416.8\ \text{kJ mol}^{-1} \tag{7}$$

Table 3
Mass balance for manganese in the Fe-GAC synthesis process.

Fe-GAC base type (Fe content)	After $KMnO_4$ pretreatment Mn in rinse as			% Mn in solid	After $FeSO_4$ treatment Total Mn in		
	Unreacted Mn as $KMnO_4$ (% of initial) A	Reduced Mn species (% of initial) B	Total Mn (% of initial) C	in Mn-GAC (% of initial) D	Rinse (% of initial) E	Fe-GAC (% of initial) F	Total recovered (% of initial) A+E+F
Lignite (~12.1%)	0.90	2.66	3.56	90.37	90.38	5.18	99.12
Bituminous (~8.5%)	18.29	8.03	26.32	74.45	67.33	0.80	94.44

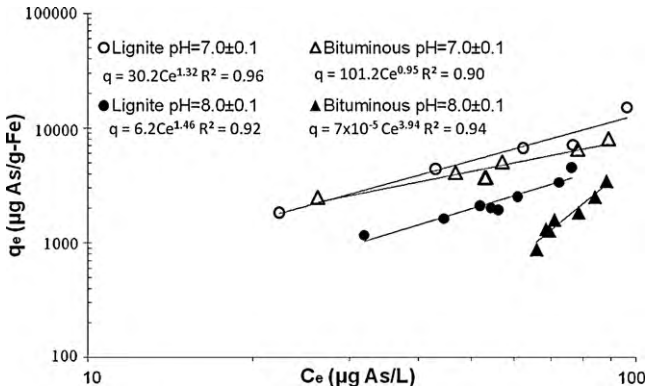

Fig. 5. Freundich equilibrium adsorption isotherms for arsenic removal by Fe-GAC (contact time 3 days; 10 mM $NaHCO_3$ buffered water; $C_{As\text{-}Initial} \approx 120\ \mu g\ L^{-1}$).

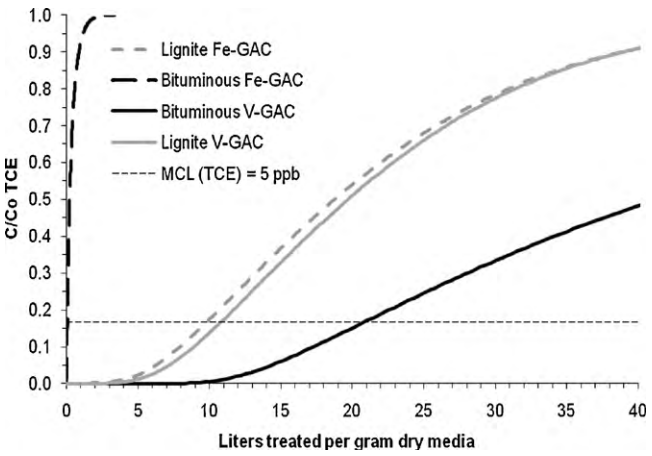

Fig. 6. TCE breakthrough predictions simulated full-scale system packed with the lignite and bituminous Fe-GAC media. ($C_{0\text{-}TCE} = 30\ \mu g\ L^{-1}$).

$$2H_2O + 2Fe^{2+} + MnO_2 \rightarrow 2FeOOH\downarrow + 2H^+ + Mn^{2+} \quad \Delta G_f^\circ = -112.2\ \text{kJ mol}^{-1} \tag{8}$$

Considering the XRD data, it is probable that the iron (hydr)oxide nanoparticles formed in the bituminous GAC via the mechanism in Eq. (7). However, in the case of lignite-based GAC, the mechanism is expected to be the one in Eq. (8). Both of these mechanisms are thermodynamically favorable under standard conditions, as expressed by the negative Gibbs free energies. In addition to the redox processes described by Eqs. (7) and (8), other oxidized manganese species likely are involved in directing the formation of the iron (hydr)oxide nanoparticles.

Nanoparticle formation may also be affected by pH. As shown in Eqs. (7) and (8), release of protons further decreased the already low pH from 2.8 to 2.5. The initial pH of 2.8 was caused by hydrolysis of the ferric ion aqueous solution, which led to a release of protons, as illustrated in Eq. (9):

$$Fe(H_2O)_6^{3+} \rightarrow Fe(OH)(H_2O)_5^{2+} + H^+ \tag{9}$$

Considering that acidic environments cause dissolution of ferric (hydr)oxide species, it may be postulated that neutralization of the generated protons would shift Eqs. (7) and (8) toward formation of more nanoparticles, which in turn would result in higher iron content in the Fe-GAC.

3.3. Removal of arsenate and trichloroethylene

The arsenic equilibrium adsorption data fitted with the Freundlich isotherm model are presented in Fig. 5. This adsorption capacity of the Fe-GAC media is expressed per mass of iron so that it can be easily compared with the adsorption capacities of other iron-containing adsorbents. The lignite-based Fe-GAC exhibited slightly higher adsorption capacity than its bituminous Fe-GAC counterpart, which could be expected considering the higher iron loading. The adsorption isotherms of the virgin GAC media were not plotted because the plain carbon did not exhibit any significant arsenic adsorption capacity.

The Freundlich adsorption intensity parameters ($1/n$) for arsenate were generally ≥ 1, with exception of the bituminous Fe-GAC, which was ~ 0.95 at pH = 7 ± 0.1 (Table 4). Values for $1/n > 1$ generally suggest unfavorable adsorption. For arsenate, this unfavorable adsorption results from the electrostatic repulsion between the prevalent $H_2AsO_4^-$ and $HAsO_4^{2-}$ species and the negatively charged carbon surface, which is dominant at these pHs [21]. The surface charge for the bituminous Fe-GAC is ~ -15 mV at pH ~ 7, while that of the lignite-based Fe-GAC is ~ -25 mV at the same pH (Fig. 4). This data correlates well with the $1/n$ values for the Fe-GAC media at this pH, i.e., $1/n$ is lower for the bituminous Fe-GAC. At pH = 7, both virgin carbon bases have surface charges of −40 mV. An increase in the iron loading should create more positively charged surfaces, which would weaken this electrostatic repulsion and create a favorable environment for adsorption ($1/n < 1$) in addition to providing more nanoparticles for sorption of arsenate. Conversely, high iron loading may also result in pore clogging and/or reduction in the net available surface area, leading to poor adsorption kinetics and fewer available sorption sites.

The Freundlich adsorption capacity parameters for arsenate (Table 4) were relatively lower than those reported for similar media [11]. This is not completely unexpected considering that high $1/n$ parameters usually cause capacity parameters to be low [21].

The Freundlich adsorption capacity and intensity parameters for TCE were very similar for the lignite-based virgin GAC and Fe-GAC media, suggesting that the synthesis method did not adversely impact the TCE adsorption capacity of the media (Table 4). For the bituminous GAC media, however, the adsorption capacity parameter decreased almost four times, from ~17 to ~4.4 (mg TCE/g)(L/mg)$^{1/n}$, while the adsorption intensity parameter increased from 0.7 to 1.7, indicating changes in the carbonaceous surface of the GAC material after the synthesis of the iron nanoparticles. This trend could be attributed to formation of nanoparticle-containing surfaces in the micropore range where the adsorption of TCE is expected to be predominant. The increase in the differential pore volume of the lignite-based Fe-GAC (Fig. 3) implies the creation of new pores of <20 nm due to deposition of nanoparticles on the GAC surfaces, as shown in Fig. 1a. These nanoparticles block the carbonaceous pores capable of adsorbing the TCE. Considering that the number of available micropores is 2–3 times higher for the lignite-based Fe-GAC than the bituminous Fe-GAC, this phenomenon does not significantly affect the overall TCE removal performance of the lignite-based Fe-GAC. The TCE removal capability of the bituminous Fe-GAC may be further hindered by the permanganate during pretreatment. Pretreatment with a strong oxidizer may cause oxidation of the carbonaceous surface and formation of carboxylic, carboxylic or hydroxyl groups, which lowers the affinity of carbonaceous media for organics such as TCE.

The effect of the nanoparticle synthesis process on the TCE removal capability of the bituminous Fe-GAC is clearly illustrated by the data presented in Fig. 6 for the predicted performance of a

Table 4
Results of adsorption isotherm testing for arsenate and TCE.

GAC	Lignite			Bituminous		
	K_A (μg/g)(μg L^{-1})$^{1/n}$	1/n	R^2	K_A (μg/g)(μg L^{-1})$^{1/n}$	1/n	R^2
Arsenate adsorption pH = 7.2 ± 0.1						
Fe-GAC	3.65	1.32	0.96	8.62	0.95	0.91
Untreated	0.00	4.13	0.12	0.00	2.45	0.64
Arsenate adsorption pH = 8.0 ± 0.1						
Fe-GAC	0.80	1.46	0.92	0.00	3.94	0.94
Untreated	0.00	2.67	0.03	2.65	0.94	0.00
TCE adsorption						
Fe-GAC	18.05	0.95	0.90	4.43	1.72	0.95
Untreated	14.54	0.87	0.95	16.97	0.70	0.81

full-scale continuous flow system. The PSDM predicted that a gram of dry virgin GAC media could treat ~7.2 L of TCE-contaminated water before the MCL for TCE would be reached. This value was close to the value of ~6.3 L g^{-1} of dry media for the lignite-based Fe-GAC, which is equivalent to a ~12.5% decrease in TCE removal capability as a result of nanoparticle synthesis. In contrast, the bituminous virgin GAC was capable of treating ~14.5 L of water per gram of dry media before the MCL for TCE was reached, whereas the bituminous Fe-GAC was capable of treating only 0.2 L of water per gram of dry media. This ~99% decrease in TCE removal capability highlights the magnitude of the effect GAC type may have on the overall contaminant removal capabilities of hybrid media such as Fe-GAC.

For arsenic, the PSMD predicted that the lignite-based Fe-GAC could treat 4 L of water per gram of dry media until the MCL for arsenate is reached, while the bituminous Fe-GAC could treat only 2.8 L of water per gram of dry media (Supplemental Information Figure S2). This was expected as the isotherm data already implied this trend. The modeled removal capacity of the bituminous Fe-GAC is ~30% lower than that of its lignite counterpart. Interestingly, the bituminous Fe-GAC contained ~30% less iron, suggesting that the iron content may be the dominant factor in determining the overall arsenic adsorption capacity of this type of media, which also exhibits differences in surface charge and surface area.

The contaminant removal performances of both media may be lower than the above-mentioned PSDM predictions if realistic water matrices (e.g. groundwater) are considered, which could contain number of other co-contaminants in addition to the arsenic and TCE. In realistic water matrices, the existing co-contaminants will compete with the arsenic and/or TCE for the limited adsorption sites. This competition could even result in desorption of arsenic or TCE, which may consequently be released in the treated effluent at higher concentrations than the ones of the influent. In this case, the magnitude of the adsorption/desorption processes (i.e. competition) will be primarily impacted by the concentrations of the competing co-contaminants and their affinity for the adsorption sites. Additionally, size exclusion effects may be exhibited by the media for larger organic co-contaminant molecules, which may not be able to access available adsorption of media as a result of pore blockage.

It is interesting to note that water matrices containing high concentration of dissolved iron could further complicate the intraparticle mass transport mechanism and adsorption of contaminants. The dissolved iron, for example, could contribute to growth of the iron (hydr)oxide nanoparticles by slow precipitation of the iron. This process could initially generate additional arsenic adsorption sites leading to prolonged complete removal of arsenic as shown in the study conducted by Khan et al. [34]. However, this process also cause serious pore clogging over a prolonged period of time; consequently leading to increase in intraparticle mass transport resistance and/or reduction in the media's ability to remove organic contaminants.

4. Conclusions

Hybrid adsorbent media may offer a viable alternative to other methods for removal from water of multiple contaminants with different chemistries. However, while synthesis of iron (hydr)oxide nanoparticles may transform GAC media into media with the ability to remove arsenic, the ability of this media to remove organic co-contaminants may seriously be reduced, as shown in this study. This tradeoff is controlled by several factors, but type and properties of the virgin GAC, which are directly related to the properties of the coal used as a raw material and its type variability, appear to play the most important role in the overall contaminant removal performance of Fe-GAC media. Even though new pores are created in the Fe-GAC, they may have different chemistries as a result of the use of strong oxidizers or different iron (hydr)oxide nanoparticle deposition mechanisms during the synthesis process. As such, these pores may have reduced ability to adsorb organic co-contaminants. Additionally, iron (hydr)oxide nanoparticles could block the existing micropores, which would consequently limit access to the surfaces capable of adsorbing organics. These limiting processes may be prevalent in microporous GAC media. In the specific example illustrated in this study, microporous bituminous GAC resulted in Fe-GAC media with poor TCE removal capability. In contrast, the ability of the macroporous lignite-based Fe-GAC media to remove TCE was not seriously reduced. Additionally, the arsenic removal ability of the lignite-based Fe-GAC media was better than that of the bituminous Fe-GAC, implying that selection of macroporous GAC media as a base material may be a more viable option for minimizing the effects of this tradeoff when synthesizing Fe-GAC media with this synthesis method.

The above-presented results clearly demonstrate that impregnation of metal (hydr)oxide nanoparticles into granulated activated carbon create much greater implications related to the overall contaminant removal than the sole improvements related to arsenic removal abilities of hybrid media. The nanoparticle impregnation facilitates changes in properties of the media, which could consequently result in a reduced ability to remove other non-competing contaminants. Therefore, when engineering nanoparticle-containing hybrid media for removal of arsenic and co-contaminants, it is imperative to examine how each step of the "hybridization" process impacts the overall performance of the new hybrid media.

Appendix A. Supplementary data

Supplementary data associated with this article can be found, in the online version, at doi:10.1016/j.jhazmat.2010.07.036.

References

[1] L. Reitner, H. Falk, C. Groat, C.M. Coussens, From Source Water to Drinking Water: A Workshop Summary, 2004, Retrieved from http://books.nap.edu/openbook.php?record_id=11142&page=47.

[2] D. Mohan, C.U. Pittman Jr., Arsenic removal from water/wastewater using adsorbents – a critical review, J. Hazard. Mater. 142 (1–2) (2007) 1–53.

[3] B.K. Mandal, K.T. Suzuki, Arsenic round the world: a review, Talanta 58 (2002) 201–235.

[4] International Agency for Research On Cancer, IARC Monographs on the evaluation of carcinogenic risks to humans: group 1 carcinogenic to humans [Fact sheet], 2008, Retrieved from http://monographs.iarc.fr/ENG/Classification/crthgr01.php.

[5] United States Department of Health Human Services (Ed.), Toxicological Profile for Arsenic, US Department of Health and Human Services, Washington, DC, 2007.

[6] D.M. Sherman, S.R. Randall, Surface complexation of arsenic (V) to iron(III) (hydr)oxides: structural mechanism from ab initio molecular geometries and EXAFS spectroscopy, Geochim. Cosmochim. Acta 67 (22) (2003) 4223–4230.

[7] G. Ona-Nguema, G. Morin, F. Juillot, G. Calas, G.E. Brown, EXAFS analysis of arsenite adsorption onto two-line ferrihydrite, hematite, goethite, and lepidocrocite, Environ. Sci. Technol. 39 (23) (2005) 9147–9155.

[8] D. Mohan, C.U. Pittman, Arsenic removal from water/wastewater using adsorbents – a critical review, J. Hazard. Mater. 142 (2007) 1–53.

[9] M. Badruzzaman, P. Westerhoff, D.R.U. Knappe, Intraparticle diffusion and adsorption of arsenate onto granular ferric hydroxide (GFH), Water Res. 38 (18) (2004) 4002–4012.

[10] K. Hristovski, P. Westerhoff, J. Crittenden, An approach for evaluating nanomaterials for use as packed bed adsorber media: A case study of arsenate removal by titanate nanofibers, J. Hazard. Mater. 156 (2008) 604–611.

[11] K.D. Hristovski, P.K. Westerhoff, T. Moller, P. Sylvester, Effect of synthesis conditions on nano-iron (hydr)oxide impregnated granular activated carbon, Chem. Eng. J. 146 (2008) 237–243.

[12] United States Environmental Protection Agency, Basic information about trichloroethylene in drinking water [web page], 2009, Retreived from http://www.epa.gov/safewater/contaminants/basicinformation/trichloroethylene.html.

[13] United States Environmental Protection Agency, EPA National primary drinking water standards [Fact sheet], 2006, Retrieved from http://www.epa.gov/safewater/contaminants/index.html#1Z.

[14] Z. Gu, J. Fang, B. Deng, Preparation and evaluation of GAC-based iron-containing adsorbents for arsenic removal, Environ. Sci. Technol. 39 (2005) 3833–3843.

[15] W. Chen, R. Parette, F.S. Cannon, Arsenic adsorption via iron-preloaded activated carbon and zero-valent iron, J. Am. Water Works Assoc. 100 (8) (2008) 96–105.

[16] B.E. Reed, R. Vaughan, L. Jiang, As(III), As(V), Hg and Pb removal by Fe-oxide impregnated activated carbon, J. Environ. Eng. 126 (9) (2000) 869–873.

[17] A.K. Sengupta, L.H. Cumbal, Method of manufacture and use of hybrid anion exchanger for selective removal of contaminating fluids, US Patent Application 20,050,156,136, July 21 (2005).

[18] M.A. Franson, A.D. Eaton, L.S. Clescri, A.E. Greenberg (Eds.), Standard Methods for the Examination of Water and Wastewater, 19th ed., American Public Health Association, Washington, DC, 1995.

[19] United States Environmental Protection Agency, Test Methods for Evaluating Solid Waste (Physical/Chemical Methods SW-846), US EPA, Washington, DC, 1996.

[20] Carus Chemical Company, Analytic method 102: determination of CAIROX potassium permanganate residual for drinking water treatment. Retrieved from Carus Chemical Corporate Website: www.caruschem.com (2004, January).

[21] H. Sontheimer, J. Crittenden, S. Summers, Activated Carbon for Water Treatment, 2nd ed., DVGW-Forschungsstelle, Engler-Bunte Institut, Universitat Karlsruhe, Karlsruhe, Germany, 1988.

[22] J.C. Crittenden, R.R. Trussell, D.W. Hand, K.J. Howe, G. Tchobanoglous, Water Treatment: Principles and Practice, 2nd ed., John Wiley and Sons, Hoboken, NJ, 2005.

[23] R.G. Zytner, Adsorption–desorption of trichloroethylene in granular media, Water Air Soil Pollut. 65 (1991) 245–255.

[24] K. Hristovski, P. Westerhoff, J. Crittenden, L. Olson, Arsenate removal by iron (hydr)oxide modified granulated activated carbon: modeling arsenate breakthrough with the pore surface diffusion model, Sep. Sci. Technol. 43 (2008) 3154–3167.

[25] D.R. Lide, CRC Handbook of Chemistry and Physics, 84th ed., CRC Press, Boca Raton, FL, 2003.

[26] V. Langer, K. Novakowski, A. Woodbury, Sorption of trichloroethene onto stylolites, J. Contam. Hydrol. 40 (1999) 1–23.

[27] D.M. LeVan, G. Carta, C.M. Yon, Adsorption and ion exchange, in: R.D. Perry, D.W. Green (Eds.), Perry's Chemical Engineers' Handbook, 7th ed., McGraw-Hill, New York, 1997 (Chapter 16).

[28] K.A. Mertz, F. Gobin, D.W. Hand, D.R. Hokanson, J.C. Crittenden, Manual: Adsorption Design Software for Windows (Ad-DesignS), Michigan Technological University, Houghton, MI, 1999.

[29] C. Tadanier, M. Schreiber, J. Roller, Arsenic mobilization through microbially mediated deflocculation of ferrihydrite, Environ. Sci. Technol. 39 (2005) 3061–3068.

[30] B. Buecker, Coal: what your parents never taught you, Power Eng. (November) (2006) 104–114.

[31] J.G. Kim, J.B. Dixon, C.C. Chusuei, Y. Deng, Oxidation of chromium(III) to (VI) by manganese oxides, Soil Sci. Soc. Am. J. 66 (2002) 306–315.

[32] A. Navrotsky, L. Mazeina, J. Majzlan, Size-driven structure and thermodynamic complexity in iron oxides, Science 319 (2008) 1635–1638.

[33] S. Parc, D. Nahon, Y. Tardy, P. Viellard, Estimated solubility products and fields of stability for cryptomelane, nsutite, birnessite, and lithiophorite based on natural lateritic weathering sequences, Am. Mineral. 74 (1989) 466–475.

[34] A.H. Khan, S.B. Rasul, A.K.M. Munir, M. Habibuddowla, M. Alauddin, S.S. Newaz, A. Hussam, Appraisal of a simple arsenic removal method for groundwater of Bangladesh, J. Environ. Sci. Health A35 (2000) 1021–1041.